ACTA CLIMATOLOGICA ET CHOROLOGICA
Universitatis Szegediensis, Tomus 49-50, 2016, 49-61

ANALYSIS OF LAND SURFACE TEMPERATURE AND NDVI DISTRIBUTION FOR BUDAPEST USING LANDSAT 7 ETM+ DATA

G MOLNÁR

Department of Climatology and Landscape Ecology, University of Szeged, P.O. Box 653, 6701 Szeged, Hungary
E-mail: molnarge@geo.u-szeged.hu

Summary: Urban areas considerably vary in land coverage, emission of pollutants and anthropogenic heat release from the natural surroundings. As a result, an alteration of meteorological variables (e.g. temperature, wind, moisture) is detected in the cities, which can fundamentally be observed with three methods: in-situ measurements, numerical mesoscale meteorological models and remote sensing products. In this work, a satellite imagery (single-channel algorithm) technique was utilized to investigate the spatial distribution of land surface temperature (LST) and normalized vegetation index (NDVI) for the capital city of Hungary. The high-resolution thermal infrared band (60 m) of Landsat 7 ETM+ (Enhanced Thematic Mapper Plus) provides a powerful tool to categorize different land cover zones and to determine the thermal properties of land surface. Two dates (2 and 18 August 2014) and 11 Local Climate Zones (LCZs) were selected to take into consideration the progress of vegetation and the dissimilarity of land coverage in LST modification. The results suggest that the presence of vegetation leads to a significant LST reduction. For instance, the thermal contrast between the LCZs of compact midrise (NDVI: 0.15) and dense trees (NDVI: 0.73) passed 40 °C on 02 August, 2014. On average, the LST approached 40 °C in case of three LCZs (compact midrise, compact low-rise, open midrise) and for 9% of the total study area.

Key words: Land surface temperature, Normalized Difference Vegetation Index, Landsat 7 ETM+, Local Climate Zones, Single-channel Algorithm, NDVI Threshold Method

1. INTRODUCTION

After the industrial revolution, the population started to increase explosively, and this process caused a rapid urbanization. Whilst 3% of the global population lived in urban areas in the 1800s, nowadays this ratio exceeds 50%. The tendency will likely continue in the forthcoming decades: according to some estimations (e.g. UN 2015), the expansion of urban areas can reach 66% by the 2050s. Urbanization contributes to the change of land-use and environmental factors. The natural landscape being replaced by artificial materials generated a remarkable change in physical features: roads, pavements have lower albedo, higher volumetric heat capacity and thermal conductivity compared to the natural sites.

The modification of the surface energy balance can also be observed in the urban areas. Because of the lower albedo, less incoming (shortwave) radiation is reflected from the ground, thus more heat (energy) is stored in the urban fabric. The reflected shortwave beam is strongly absorbed and backscattered by the pollutants. Long wave components are also attenuated by the absorbtion and re-emission of the aerosol particles. Traffic, industry, domestic energy usage (heating, cooling, cooking etc.) induces a large quantity of anthropogenic heat (AH) emission. Emission of stored and anthropogenic heat leads to an

energy surplus in the inner cities. Subsequently, a temperature difference occurs between the urban and rural areas, which is named the urban heat island (UHI) phenomenon. As reported by most studies (e.g. Miao et al. 2009, Wang et al. 2013, Chen et al. 2014), the proportion of AH release in a heat island may attain 30% depending on the land cover categories.

UHI is mostly developed under anticyclonic synoptic conditions, when the wind speed is low and the insolation is not interrupted by clouds. As a result of complex physical processes, the magnitude and the behavior of vertical heat island are diversified in the urban boundary layer. Features of the surface heat island (SUHI) depend on the amount of incoming radiation, hence the largest intensities can be found in summer at daytime, while the conventional (canopy layer) heat island is strongest at nighttime due to the heat emission from artificial materials. The frequency of heat waves tends to be higher in the forthcoming decades (Field et al. 2014). The existing heat island increases, even more enhancing the thermal load during the heat wave periods proportionally to the city-size (Gosling et al. 2007). The other significant environmental problem is the photochemical transformation of precursors (e.g. nitrogen-oxides, carbon monoxide, VOC). Consequently, the mortality rate of urban habitants becomes larger afterwards (WHO 2004), which urges the decision-makers to assign a reason to mitigation strategies. One of the most productive approach is the establishment of green areas. Vegetation lowers the temperature by the shading effect and reduces the air pollution by the stomatal exchange of CO_2/O_2. By the biophysical process of evapotranspiration, plants distract latent heat from the environment cooling their local area as well. Besides these direct effects, the greenery lowers the emission of pollutants by decreasing the energy consumption of AC systems. The advancement of remote sensing has opened a new dimension in the urban environment- and vegetation-related investigations. Nowadays, large datasets are available for scientific and educational purposes, because the satellites guarantee high-resolution and continuous data even where field observations are not applicable or do not exist.

Numerous researches examine the connection between the NDVI and the LST using Landsat 7 ETM+ data. Mallick et al. (2008) found reasonably strong relationship between the two variables. The land cover category of dense vegetation (forest) and high dense built-up showed the highest (R^2=-0.752) and the lowest (R^2=-0.394) correlation in Delhi (India). Alipour et al. (2008*)* compared the mono-window algorithm of Qin et al. (2001) and the single-channel method of Jimenez-Munoz and Sobrino (2003). The results argued that both algorithms captured the LST distribution well with an irrelevant difference ($\Delta R^2 \approx 0.06$). Senanayake et al. (2013) introduced the Environmental Criticality Index (ECI) based on the ratio of LST and NDVI. ECI presented inverse proportion to NDVI, thus the areas with lack of vegetation might have high 'environmental criticality'. Walawender et al. (2014) confirmed that the land-cover characteristics (e.g. shape of buildings, availability of vegetation) are the most decisive circumstances in the spatial distribution of LST. They emphasized that the largest influence on LST can be observed at the end of the vegetation period, when the greenery is greatly developed.

Urban environment research has been conducted in Budapest since the 1970s (Probáld 1974, 2014). The studies have generally been focused on the comparison of in-situ measurements and satellite observations. In the work of Pongrácz et al. (2010), a Terra/MODIS (Moderate Resolution Imaging Spectroradiometer) dataset was employed to study the thermal conditions in Budapest and other Central European cities (e.g. Belgrade, Bucharest, Milan, Munich, Sofia, Vienna, Warsaw, Zagreb). The largest SUHI appeared in summer at nighttime; the monthly mean values reached 3–4 °C in Budapest. Fricke et al.

(2014) investigated the relationship between LST and vegetation-cover on the district-scale. MODIS measurements indicated that the SUHI was, on average, 1.5–2 °C higher in the urbanized territories than in the encircling forests. Gábor and Jombach (2009) classified the land surface of Budapest into 14 classes and calculated LST and NDVI using Landsat 5 TM. The study showed that the highest LSTs were found in the categories of Intensive residential, Commercial and railway junctions. In addition, the average temperature difference achieved 14 °C between Woodland and Commercial classes.

The main objective of our investigation is to analyze the role of greenery in thermal load reduction by the comparison of NDVI and LST distribution in Budapest. To the best of the author's knowledge, Landsat 7 ETM+ data have not been applied to similar investigations yet, therefore this work aims to provide a beneficial basis for further research. In this study, after a short review of urban environment, the study area and the operation of Landsat 7 ETM+ are described in Section 2. Then the article gives a short explanation about the calculation of NDVI and LST using the images of red, near infrared and thermal infrared bands. Finally, maps and cross-section diagrams are represented to understand the spatial pattern of NDVI and LST distribution for the 11 Local Climate Zones (LCZs) (Stewart and Oke 2012) of Budapest.

2. MATERIALS AND METHODS

2.1. Description of the study area

Budapest (47,5°N, 19°E) is located in the Carpathian Basin in the northern part of Hungary with an area of 525.2 km^2. 1.76 million people have been living in the largest city of Hungary recently, but the population has decreased by 10% in the last 2 decades (Census of Hungary 2013). Budapest is surrounded by Pilis Mountainss and Szentendre Island in the north, Pesti Plain and Gödöllő Hills in the east, Csepel Island in the south and Tétény Uphill and Buda Hills in the west. The river Duna splits the city into two parts and creates the Óbuda Island, Margaret Island, Csepel Island. Buda Hills, the westernmost part of the study area contain steep hills (the highest point is 528 m), whilst on the east side of Duna River the relief is insignificant. The climate of Budapest is Cfb (Maritime temperate) and Dc (Temperate continental) according to Köppen and Trewartha (Köppen 1923, Peel et al. 2007) with a mean annual temperature and a precipitation of 11.3 °C and 533 mm, respectively.

11 Local Climate Zones were distinguished on the basis of the land cover of Budapest, following the work of Stewart and Oke (2012). This technique is based on uniform geometric (sky view factor, aspect ratio, building surface fraction, impervious surface fraction, natural surface fraction, pervious surface fraction, height of roughness elements, terrain roughness class) and thermal/radiative/metabolic (surface admittance, surface albedo, anthropogenic heat output) properties of a local (few kilometer expanse) area. The LCZ technique employs three aspects during the classification process (built types, land cover types, variable land cover properties) creating 20 categories (see more in Stewart and Oke 2012). Budapest was classified into 11 LCZs (Table 1) of which the largest is the LCZ of large low-rise (25.9%). The historical city center and its narrow environment are dominated by commercial and residential buildings with continuous urban fabric (compact midrise, compact low-rise). Large low-rise, open midrise and open low-rise categories are located in the outer residential belt, where the vast majority of the population lives. The southeastern and the southwestern

part of the city includes meadows, arable lands and agricultural areas (low plants, bare soil). The largest continuous forests are placed in the Buda Hills (dense trees), and remarkable vegetation is found in the major parks of Budapest (scattered trees: Orczy-park, Népliget, Városliget).

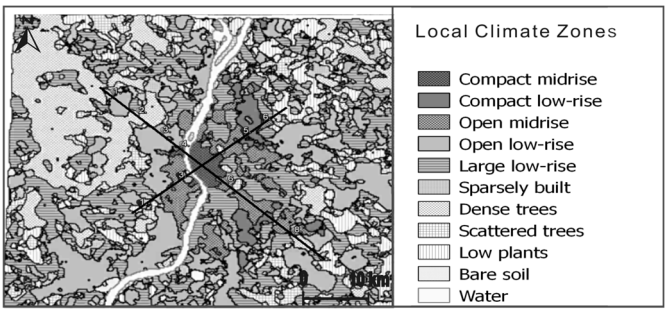

Fig. 1 Spatial distribution of the LCZs and the situation of the northwest-southeast and southwest-northeast cross-sections (detailed in Chapter 3.3.) in Budapest. The markers denote those places that have been numbered in Fig. 4 and Fig. 5

Table 1 Extension of the Local Climate Zones in Budapest

LCZ	LCZ name	Percentage of area
LCZ 2	compact midrise	1.1
LCZ 3	compact low-rise	2.4
LCZ 4	open midrise	5.6
LCZ 5	open low-rise	19.7
LCZ 8	large low-rise	25.9
LCZ 9	sparsely built	6.3
LCZ A	dense trees	15.2
LCZ B	scattered trees	9.6
LCZ D	low plants	10.5
LCZ F	bare soil	1.1
LCZ G	water	2.9

2.2. Description of the meteorological data and the Landsat 7 ETM+ satellite

As a result of the USGS (United States Geology Survey) data policy, Landsat 7 data can be downloaded free of charge since 1 October, 2008. The images are geometrically and radiometrically corrected in order to take the geolocation and the systematic (sensor) errors into account. In order to represent the urban effect and the peak period of vegetation, two distinct dates were chosen (2 and 18 August 2014). On both days, high-pressure formation dominated the Carpathian Basin. The maximum of 2-m temperature exceeded 25 °C (2 August: 31.9 °C; 18 August: 25.4 °C) and no precipitation occurred. The low cloud fraction (0 octa during the observations) favored for high insolation, therefore strong SUHI could be formed.

The Landsat satellites were constructed to satisfy various scientific interests in the field of agriculture, forestry, geology and meteorology. They have been operating since 1972, when the Landsat 1 was launched. Data acquisition of Landsat 7 has been started on 15 April 1999 on-board with the ETM+ (Enhanced Thematic Mapper Plus) sensor. Landsat 7 is on sun-synchronous orbit (inclined 98.2°) and supplies a temporal resolution of 16 days. ETM+

was originally developed for Landsat 6 and contains several improvements compared to the previous sensor (TM – Thematic Mapper; Landsat 4 and Landsat 5). This sensor possesses a new panchromatic band and a refined thermal infrared band with the spatial resolutions of 15 m and 30 m respectively and it consists of eight bands altogether. The scan line corrector (SLC) of ETM+ malfunctioned on 31 May 2001 resulting data-free black strips at the edge of images and about 22% data-loss for each pass (Chandler et al. 2009). A large number of methods (Storey et al. 2005 Zhang et al. 2007, Zeng et al. 2013) were constructed in order to recover missing pixels (e.g. kriging local histogram comparison method, weighted linear regression method, triangulation method) based on statistical comparison of the existing and the absent values.

2.3. Calculation of NDVI and LST

First, every pixel from the downloaded images was converted from DN (digital number) to spectral radiance (L_λ) in order to receive measurable physical quantities Eqs. 1, 2, 3. Before the calculation of spectral radiance, the theoretical maximum and minimum of digital numbers and spectral radiances have to be estimated with post-calibration creating the gain (G) and the bias (B) parameters.

$$G = \frac{L_{\max\lambda} - L_{\min\lambda}}{DN_{\max} - DN_{\min}} \tag{1}$$

$$B = L_{\min\lambda} - G \cdot DN_{\min} \tag{2}$$

$$L_\lambda = G \cdot DN - B \tag{3}$$

In order to determine the NDVI, the spectral radiance has to be converted into spectral reflectance (4) by employing the following equation for the red (0.631–0.692 μm) and the near infrared bands (0.772–0.898 μm):

$$\rho_\lambda = \frac{\pi \cdot L_\lambda \cdot d^2}{E_{SUN\lambda} \cdot \sin(\Theta_s)} \tag{4}$$

The sun elevation angle (Θ_s), the mean solar irradiance and the mean Sun-Earth distance (d) were obtained from metadata. The vegetation reacts separately for the different wavelength of electromagnetic radiation. The leaf pigments (chlorophyll) absorb the red (and the blue) portion of visible spectrum, while the near infrared part is reflected. It is worth noting that the phenological phase and the environmental conditions (heat and moisture stress) are primary factors in shaping the rate of reflection. In autumn, the leaves reflect less NIR (and more visible) radiation than in spring. Myriads of investigations (Jordan 1969, Rousse et al. 1974, Gitelson 2004) aimed to capture the step of reflection at the border of NIR and red spectrum of electromagnetic radiation. One of the most common index is NDVI, which can be estimated with this expression:

$$NDVI = \frac{\rho_{NIR} - \rho_{RED}}{\rho_{RED} + \rho_{NIR}} \tag{5}$$

The land surface emissivity (6) expresses the ability of thermal energy emission for a given material, thus this parameter is required to calculate the land surface temperature. Since

both the NDVI and the LSE are interpreted as a characteristic of land cover, the emissivity can be predicted with this vegetation index producing the so-called NDVI Threshold Method (hereinafter THM) (Sobrino et al. 2004). THM uses predetermined values of emissivity and NDVI for soil ($\varepsilon_{s\lambda}$=0.92, $NDVI_s$=0.2) and vegetation ($\varepsilon_{v\lambda}$=0.99, $NDVI_v$=0.5). To take the water and urban surfaces into consideration, new LSE values (ε_w=0.96, ε_u=0.92) were introduced.

$$\varepsilon_\lambda = \begin{cases} \varepsilon_{s\lambda} & NDVI < NDVI_s \\ \varepsilon_{s\lambda} + (\varepsilon_{v\lambda} - \varepsilon_{s\lambda}) P_v & NDVI_s < NDVI < NDVI_v \\ \varepsilon_{v\lambda} & NDVI < NDVI_v \end{cases} \quad (6)$$

The P_v term (7) is the fractional vegetation cover on mixed land cover areas (Carlson and Ripley 1997), and ranging from 0 ($NDVI=NDVI_s$) to 1 ($NDVI=NDVI_v$):

$$P_v = \left(\frac{NDVI - NDVI_s}{NDVI_v - NDVI_s} \right)^2 \quad (7)$$

Sobrino et al. (2008) found that the THM underestimates the emissivity of water, snow, ice and rocks. To consider the limitation of method for water bodies, a new emissivity value (0.97) was set, when NDVI is less than -0.3. Besides the THM, the TES (Temperature emissivity separation; Gillespie et al., 1998) and the TISI (Temperature independent spectral indices; Becker and Li 1990) algorithms are also valuable tools to compute the LSE. Oltra-Carrió et al. (2012) analyzed the land surface temperature pattern with different emissivity estimations for grass, bare soil and artificial surfaces and showed that the TES (RMSE=1.6 K) and the TISI (RMSE=1.7 K) performed better than the THM (RMSE=2.3 K). Nevertheless, the TES can only be used with at least four TIR image, and the TISI is designed with observations from daytime and nighttime, therefore the THM tends to be the most suitable method in our case.

Several methods were designed to calculate LST temperature by using satellite observations such as the single-channel algorithm (Jiménez-Munoz and Sobrino 2003), the mono-window algorithm (Qin et al. 2001), the split-window algorithm (Qin and Karnieli 1999) and the dual-angle method (Gu and Gillespie 2000). In this study, the single-channel algorithm (hereinafter SC) was applied, because this method does not employ such atmospheric parameters as water vapor content, effective mean temperature or at least 2 thermal bands like the mono-window and split-window algorithms. Only three parameters (band average atmospheric transmission, effective bandpass downwelling and upwelling radiance) are required for SC, which are provided by the MODTRAN atmospheric correction parameter calculator (Barsi et al. 2003). The MODTRAN claims the date (in YMDM format) and the location (latitude, longitude) compulsorily, since the surface conditions (e.g. altitude, air temperature, pressure and relative humidity) may be given optionally. If the surface conditions are not available, the values are interpolated from the observations of NCEP (National Center for Environment Prediction).

To derivate the surface temperature with SC, first, the brightness (or at-sensor) temperature (T_B) can be computed by inverting the Planck's Function:

$$T_B = \frac{K_2}{\ln\left(\frac{K_1}{L_\lambda} + 1\right)} \tag{8}$$

where K_1 (666.09 W m^{-2} sr^{-1} μm^{-1}) and K_2 (1282.71 K) are Landsat 7-specific calibration constants. In the next step, the MODTRAN outputs are used to determine ψ_1, ψ_2, ψ_3 atmospheric functions and γ, δ parameters as follows:

$$\psi_1 = \frac{1}{\tau} \tag{9}$$

$$\psi_2 = -L^{\downarrow} - \frac{L^{\uparrow}}{\tau} \tag{10}$$

$$\psi_3 = L^{\downarrow} \tag{11}$$

$$\gamma = \left\{ \frac{c_2 L_\lambda}{{T_B}^2} \left[\frac{\lambda^4 L_\lambda}{c_1} + \frac{1}{\lambda} \right] \right\}^{-1} \tag{12}$$

$$\delta = -\gamma \cdot L_\lambda + T_B \tag{13}$$

where c_1 (1.19104 10^8 W μm^4 m^{-2} sr^{-1}) and c_2 (1.43877 10^4 μm K) are constants and λ is the effective wavelength of Landsat 7 for band 6 (λ=11.27 μm) (NASA 2015). Finally, the equation of land surface temperature can be obtained:

$$T_S = \gamma \left[\frac{1}{\varepsilon} \left(\psi_1 L_\lambda + \psi_2 \right) + \psi_3 \right] + \delta \tag{14}$$

3. RESULTS

3.1. NDVI distribution patterns and quantitative results

On the two distinct dates (2 and 18 August 2014), the NDVI distribution indicated a positive gradient from the downtown (0.1–0.3) to the suburb (0.4–0.6), where the compact built-up structure is replaced with detached houses, in addition, the presence of natural surfaces becomes dominant (Fig. 2). The inner districts (e.g. Terézváros, Józsefváros, Ferencváros, Lipótváros) are characterized by the lowest NDVI (around 0.1), while areas with higher elevation (e.g. Buda Hills) and larger forests showed greater values (around 0.6). Green spots in the inner city, with a typical NDVI value of 0.5, refer to the major parks (e.g. Népliget, Városliget, Orczy-park) and recreational areas of Budapest (e.g. Margaret Island, Gellért Hill). Transport junctions, logistic centers, industrial territories are responsible for the isolated low-valued points in the suburb. Despite the similarities between the two dates, the vegetation reached the peak of its phenologic phase and biological activity on 2 August, accordingly higher NDVI were calculated at this time.

This assumption is confirmed by the NDVI values for the 11 LCZs, shown in Table 2. On 2 August, the average NDVI was 0.44, which is 16% higher than on 18 August (0.37).

The land cover zone of compact midrise indicated the lowest NDVI values (0.15 and 0.02) due to the presence of dense and large buildings and high impervious surface fraction. On the other hand, the greatly vegetated areas such as dense trees (0.73 and 0.70) or scattered trees (0.61 and 0.58) presented the highest NDVI. Areas with high NDVI can be interpreted as the most homogeneous region of Budapest based on the standard deviation rates (e.g. dense trees 0.09 and 0.11). Contrarily, the transitional categories (e.g. open low-rise, large low-rise) displayed the most complex land features (standard deviations: 0.12 and 0.16 for open low-rise; 0.18 and 0.23 for large low-rise) due to the mixture of medium-density residential and natural surfaces.

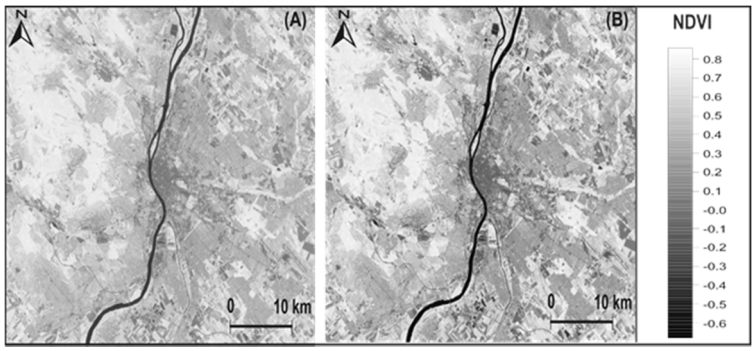

Fig. 2 Spatial distribution of the Normalized Difference Vegetation Index in Budapest on 2 (a) and 18 (b) August 2014

Table 2 Mean and standard deviation of NDVI in 11 Local Climate Zones of Budapest on 2 and 18 August 2014

LCZ name	02.08.2014.		18.08.2014.	
	Mean	Std. dev.	Mean	Std. dev.
compact midrise	0.15	0.11	0.02	0.14
compact low-rise	0.38	0.09	0.28	0.12
open midrise	0.39	0.13	0.31	0.16
open low-rise	0.47	0.12	0.39	0.16
large low-rise	0.46	0.18	0.39	0.23
sparsely built	0.55	0.12	0.50	0.16
dense trees	0.73	0.09	0.70	0.11
scattered trees	0.61	0.14	0.58	0.17
low plants	0.54	0.13	0.51	0.17
bare soil	0.48	0.20	0.40	0.25
water	0.07	0.38	-0.11	0.49

3.2. Distribution of land surface temperature

The 30-m resolution of the thermal band enables to determine the spatial pattern and the magnitude of the LST distribution in Budapest. It is clearly seen in Fig. 3 that the diversity of surface geometry generates a 30 °C interval in LST temperature on 2 and 18 August as well. The historical city center suffers a significant heat surplus because of high building and impervious surface fraction. By increasing the natural surface fraction, the surface temperature decreases rapidly, therefore the lowest LST can be found in the woodlands of

Buda Hills and in the outer districts. The local parks act as oases with high LST gradient along their border creating an ideal venue for recreational and leisure activities. Islands of Budapest (e.g. Margaret Island, Csepel Island) are also designated as cold spots for the sake of higher natural surface fraction and the cooling effect of the River Danube. The higher LSTs occurred on 2 August, when the maximum of 2-m temperature was the greatest as stated in the Bulletin of Hungarian Meteorological Service (Table 2). By this time, the thermal contrast decreased between the different land cover categories. It is worth pointing out that the LST values remained lower during the pass time of satellite in the downtown. Partly, this effect may likely be explained by the shading effect of high buildings. On the other hand, the relatively lower sun elevation angle could not let the surface being heated-up as much as on the previous date.

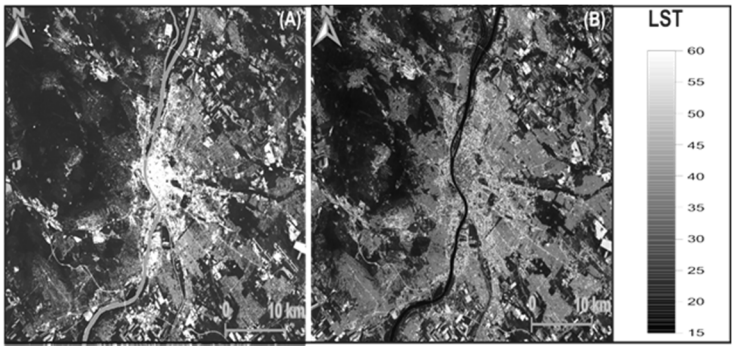

Fig. 3 Spatial distribution of the land surface temperature (LST; °C) in Budapest on 2 (a) and 18 (b) August 2014

The quantitative results suggest that the highest LST was 50–60 °C provoking a vast thermal load for the LCZ of compact midrise (Table 3). Compact low-rise (40.8 °C and 40.6 °C) and open midrise (40.0 °C and 38.6 °C) LCZs are also separated from the other groups due to their higher thermal exposure (Table 4). The substantially larger, but less populated classes like open low-rise (33.2 °C and 34.4 °C) and large low-rise (35.9 °C and 33.4 °C) were less affected by the high LST. Decrease of the impervious surface fraction delays the run-off, enhances the evaporation, the heat capacity and the albedo, and hence contributes to a huge (surface) temperature alteration. As a result of these impacts, the LST was about 40 °C lower in dense trees category on 2 August compared to the compact midrise class. The cooling potential of the three vegetation-related LCZs (dense trees, scattered trees, low plants) attained 12 °C and 9.43 °C on both dates, in contrast with the other 7 categories (except for the water class). After all, it must be highlighted that the green areas and parks not only play a role in urban planning, but also reduce the LST.

3.3. Cross-section diagrams of the land surface temperature

The LST maps extended for the entire city (or the study area) do not always give back the topographical aspect of the thermal field, so cross-section diagrams have to be created to analyze the cold and hot spots in Budapest (Fig. 1). Actually, we tried to concentrate on the first date (2 August), when the SUHI proved to be the most pronounced. The cross-sections move along a 29 km (20 km) long line from northwest to southeast (from southwest to northeast) by hitting 8 (6) well-separated area of the city.

Starting from northwest (Fig. 4), Pesthidegkút consists of medium-density residential areas, and characterized by an LST of about 25 °C, then the relief is dominated by the greatly vegetated Buda Hills, where the surface temperature decreased further (23 °C). A significant increase occured in Törökvész (30 °C) and Országút (35.1 °C) due to the existence of high-density residential and commercial areas. The maximum of LST together with the maximum of impervious and building surface fraction and the minimum of natural surface fraction produced a notable thermal load in the downtown (e.g. Lipótváros, Erzsébetváros). The equable course of LST dropped to up to 20–25 °C in the middle of the 'downtown' domain as a result of a large green space, called Szabadság Square. The same processes can be considered in Outer Ferencváros (e.g. Népliget Park at about 17.5 km), where housing estates, row housing, panel blocks and parks made the landscape diversified with approximately a 30 °C variation in LST. The external parts of southeast Budapest (Kispest, Pestszentlőrinc) displayed a decreasing magnitude of the thermal field.

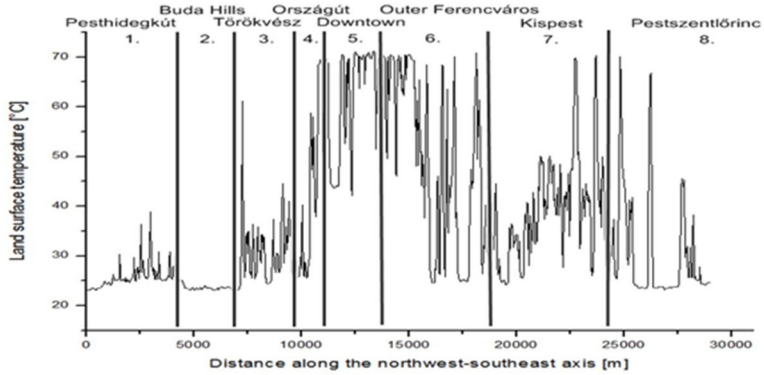

Fig. 4 Cross-section diagram of the land surface temperature along the northwest-southeast direction (02.08.2014. 09:30:53 UTC). The numbers (from 1 to 8) refer to the location of each places marked in Fig. 1

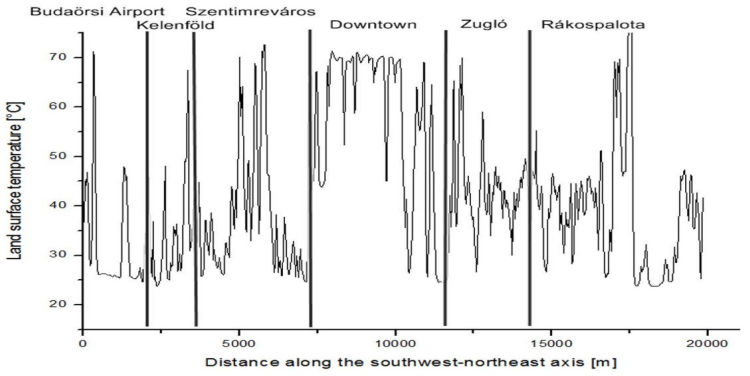

Fig. 5 Cross-section diagram of the land surface temperature along the southwest-northeast direction (02.08.2014. 09:30:53 UTC). The numbers (from 1 to 6) refer to the location of each places marked in Fig. 1

Similar to our previous case, an increasing trend is outlined along the southwest-northeast axis to the end of Downtown (Fig. 5) (Budaörsi Airport: 32.2 °C, Kelenföld: 33.5 °C, Szentimreváros: 37.9 °C, Downtown: 58.3 °C). The line, however, crosses cold spots such as the foreground of Sas Hill (at about 4.5 km) and Gellért Hill (at about 7000 m). Zugló consists of two major land cover zones: open midrise (housing estates, apartments, panel blocks) and open low-rise (family housing) resulting in a bimodal LST distribution. Rákospalota indicates a nearly constant value of LST, though the panel blocks (at about 17,000 m) trap the heat intensely during the summer months and consequently contribute to a huge thermal load. Based on the results of the two cross-sections, it is evident that the most decisive factor in the governing of the thermal field is the natural surface fraction and the elevation in Budapest.

4. CONCLUSIONS

In this study, the relationship of land-use and land surface temperature was examined using fine-resolution Landsat 7 ETM+ images taken on 2 and 18 August 2014 in Budapest. It is well known that intense urbanization and anthropogenic activity (e.g. transportation, industry, heating/cooling) generate a special climate on the meso- and microscales. The vegetation attenuates this environmental influence by shading, as well as a higher albedo and evapotranspiration related to the artificial surfaces. The goal of this analysis was to quantify the impact of greenery on LST reduction and to explore the cold and hot spots in the 11 Local Climate Zones (Stewart and Oke 2012) of Budapest. The NDVI values indicated a positive gradient towards the external areas. On 2 and 18 August 2014, the lowest NDVI was found in the LCZ of compact midrise with 0.15 and 0.02, respectively, while the dense trees category showed the highest (0.61 and 0.70) values. Due to the less phenologic development of the vegetation on the later date, NDVI, on average, decreased by 15% between the two observations. In three LCZs (compact midrise: 63.5 °C and 38.2 °C; compact low-rise: 40.8 °C and 40.6 °C; open midrise: 40.0 °C and 38.6 °C), the LST exceeded 40 °C at most times inducing a pronounced thermal field. Contrarily, the external areas (e.g. woodlands, meadows, agricultural parcels) and parks diminished the LST up to 25–35 °C. The results suggest that the thermal contrast between areas with different natural/building surface fraction became lower, when the meteorological conditions favoured a greater LST. Overall, it has to be noted that the LST alteration is primarily driven by the fraction of natural, impervious and building surfaces. Cross-section diagrams reveal that the magnitude of LST was higher in the Buda side in case of identical elevation as a result of the enhanced natural surface fraction. On the other hand, the territories on the Pest side have more complex surface structures, consequently the course of LST presents a large variety within a narrow region. Nevertheless, the importance of vegetation in LST reduction essentially depends on the season of the year, the period of the day and the location of the study area, thus our analysis cannot be generalized, but provides only site-specific information about the thermal field of Budapest.

REFERENCES

Alipour T, Sarajian MR, Esmaely A (2011) Land surface estimation from thermal band of Landsat sensor, case study: Alashtar city. Int Arch Photogramm Remote Sens Spat Info Sci 38/C7

Barsi JA, Barker JL, Schott JR (2003) An atmospheric correction parameter calculator for a single thermal band earth-sensing instrument. Proc IEEE IGARSS, 21–25 July 2003, Toulouse, France, 3014-3016.

Becker F, Li ZL (1990) Temperature-independent spectral indices in thermal infrared bands. Remote Sens Environ 32:17-33

Carlson TN, Ripley DA (1997) On the relation between NDVI, fractional vegetation cover and leaf area index. Remote Sens Environ 62:241-252

Census of Hungary (2013): 2011. évi népszámlálás. Területi adatok. [Census of Hungary (2011). Local data. (in Hungarian)] Budapest

Chandler G, Markham BL, Helder SL (2009) Summary of current radiometric calibration coefficients for Landsat MSS, TM, ETM+ and EO-1 ALI sensors. Rem Sens Environ 113:893-903

Chen F, Yang X, Zhu W (2014) WRF simulations of urban heat island under hot-weather synoptic conditions: The case study of Hangzhou City, China. Atmos Res 138:364-377

Cristóbal J, Jiménez-Munoz JC, Sobrino JA, Ninyerola M, Pons X (2009) Improvements in land surface temperature retrieval from the Landsat series thermal band using water vapor and air temperature. J Geophys Res 114:1-16

Field CB, Barros VR, Dokken DJ, Mach KJ, Mastrandrea MD, Bilir TE, Chatterjee M, Ebi LK, Estrada YO, Genova RC, Girma B, Kissel ES, Levy AN, MacCracken S, Mastrandrea PR, White LL (2014) Climate Change 2014 Impacts, Adaptation, and Vulnerability. Part A: Global and Sectoral Aspects. Contribution of Working Group II to the Fifth Assessment Report of the Intergovernmental Panel on Climate Change. Cambridge University Press, Cambridge, New York

Fricke C, Pongrácz R, Dezső Zs, Bartholy J (2014) A vegetáció szerepe a budapesti városi hősziget jelenségben. [The role of vegetation in urban heat phenomenon in Budapest (in Hungarian)]. Légkör 59:150-153

Gábor P, Jombach P (2009) The relation between the biological activity and the land surface temperature in Budapest. Appl Ecol Env Res 7:241-251

Gillespie AR (1985) Lithologic mapping of silicate rocks using TIMS. Proc TIMS Data Users' Workshop, Berkeley, CA

Gitelson AA, Kaufman YJ, Merzlyak MN (1996) Use of a green channel in remote sensing of global vegetation from EOS-MODIS. Remote Sens Environ 58:289-298

Gosling SN, McGregor GR, Páldy A (2007) Climate change and heat-related mortality in six cities. Part 1: Model construction and validation. Int J Biometeorol 51:525-540

Gu D, Gillespie AR (2000) A new approach for temperature and emissivity separation. Int J Remote Sens 21:2127-2132

Jordan CF (1969) Derivation of leaf-area index from quality of light on forest floor. Ecology 50:663-666

Ichinose T, Shimodozono K, Hanaki K (2009) Impact of anthropogenic heat on urban climate in Tokyo. Atm Environ 33:3897-3909

Jimenez-Munoz JC, Sobrino JA (2003) A generalized single-channel method for retrieving land surface remote sensing data. J Geophys Res 108:1-9

Jiménez-Munoz JC, Cristóbal J, Sobrino JA, Sória G, Ninyerola M, Pons X (2009) Revision of the single-channel algorithm for land surface temperature retrieval from Landsat thermal-infrared data. IEEE T Geosci Remote 47:339-349

Köppen W (1936) Das geographische System der Klimate. In: Köppen W, Geiger R (eds): Handbuch der Klimatologie. Verlag von Gebrüder Borntraeger, Berlin

Mallick J, Kant Y, Bharat BD (2008) Estimation of land surface temperature over Delhi using Landsat-7 ETM+. J Ind Geophys Un 12:131-140

Miao S, Chen F, LeMone MA, Tewari M, Li Q, Wang Y (2009) An observational and modeling study of characteristics of urban heat island and boundary layer structures in Beijing. J Appl Meteorol Clim 48:484-501

NASA (2015) Landsat 7 Science Data Users Handbook. National Aeronautics and Space Administrati on http://landsathandbook.gsfc.nasa.gov/pdfs/Landsat7_Handbook.pdf [accessed Dec 2015]

Oltra-Carrió R, Sobrino JA, Franch B, Nerry F (2012) Land surface emissivity retrieval from airborne sensor over areas. Rem Sens Environ 123:298-305

Peel MC, Finlayson BL, McMahon TA (2007) Updated world map of the Köppen-Geiger climate classification. Hydrol Earth Syst Sc 11:1633-1644

Pongrácz R, Bartholy J, Dezső Z (2006) Remotely sensed thermal information applied to urban climate analysis. Adv Sp Res 37:2191-2196
Pongrácz R, Bartholy J, Dezső Z (2010) Applications of remotely sensed information to urban of Central European cities. Phys Chemistry Earth 35:95-99
Probáld F (1974) Budapest városklímája [Urban climate of Budapest (in Hungarian)]. Akadémiai Kiadó, Budapest
Probáld F (2014) The urban climate of Budapest: past, present and future. Hun Geogr Bull 63:69-79
Qin Z, Karnieli A (1999) Progress in the remote sensing of land surface temperature and ground emissivity using NOAA-AVHRR data. Int J Rem Sens 20:2367-2393
Qin Z, Karnieli A, Berliner P (2001) A mono-window algorithm for retrieving land surface temperature from Landsat TM and its application to the Israel-Egypt border. Int J Rem Sens 22:3719-3746
Rouse JW, Haas RH, Schell JA Jr, Deering DW (1974) Monitoring vegetation systems in the Great Plains with ERTS. Third ERTS-1 Symposium Washington, DC, NASA, 309-317
Stewart ID, Oke TR (2012) Local Climate Zones for urban temperature studies. Bull Amer Meteor Soc 93:1879-1900
Senanayake IP, Welivitiya WDDP, Nadeeka PM (2013) Remote sensing based analysis of urban heat islands with vegetation cover using Landsat-7 ETM+ data. Urb Clim 5:19-35
Sobrino JA, Caselles V, Becker F (1999) Significance of the remotely sensed thermal infrared measurements obtained over a citrus orchard. ISPRS J Photog Rem Sens 44:343-354
Sobrino JA, Raissouni N, Li ZL (2001) A comparative study of land surface emissivity retrieval from NOAA data. Remote Sens Environ 75:256-266
Sobrino JA, Jiménez-Munoz JC, Paolini L (2004) Land surface retrieval from Landsat 5 TM. Remote Sens Environ 90:434-440
Sobrino JA., Jiménez-Munoz JC, Sória G, Romaguera M, Guanter L (2008) Land surface emissivity retrieval from different VNIR and TIR sensors. IEEE Trans Geos Rem Sens 46:316-327
Storey J, Scaramuzza P, Schmidt G, Barsi J (2005) Landsat 7 scan line corrector-off gap-filled product development. Proceedings of Pecora 16 Global Priorities in Land Remote Sensing. Sioux Falls, South Dakota
UN (2015) World Urbanization Prospects: The 2014 Revision. United Nations, Department of Economic and Social Affairs, Population Division
Walawender JP, Szymanowszki M, Hajto MJ, Bokwa A (2014) Land surface temperature patterns in the urban agglomeration of Krakow (Poland) derived from Landsat-7/ETM+ data. Pure Appl Geophys 171:913-940
Wang M, Yan X, Liu J, Zhang X (2013) The contribution of urbanization to recent extreme heat events and potential mitigation strategy in the Beijing–Tianjin–Hebei metropolitan area. Theor Appl Climatol 114:407-416
WHO (2004) Comparative quantification of health risks. Global and regional burden of disease attributable to selected major risk factors (Vol. I.). World Health Organization, Hong Kong
Zeng C, Shen H, Zhang L (2013) Recovering missing pixels for Landsat ETM+ SLC-off imagery using multi-temporal regression analysis and a regularization method. Remote Sens Environ 131:182-194
Zhang C, Li W, Travis D (2007) Gaps-fill of SLC-off Landsat ETM+ satellite image using a geostatistical approach. Int J Rem Sens 28:5103-5122